Operculo-Insular and Anterior Cingulate Plasticity Induced by Transcranial Magnetic Stimulation in the Human Motor Cortex: A Dynamic Casual Modelling Study

Duncan J. Hodkinson[1,2,3,4]*, Andreas Bungert[2], Richard Bowtell[2], Stephen R. Jackson[5], JeYoung Jung[5]*

[1] *Division of Clinical Neuroscience, School of Medicine, University of Nottingham, Nottingham, England, UK*

[2] *Sir Peter Mansfield Imaging Centre, School of Medicine, University of Nottingham, Nottingham, England, UK*

[3] *National Institute for Health Research (NIHR), Nottingham Biomedical Research Centre, Queens Medical Center, Nottingham, England, UK*

[4] *Versus Arthritis Pain Centre, University of Nottingham, Nottingham, England, UK*

[5] *School of Psychology, University of Nottingham, Nottingham, England, UK*

***Corresponding Authors**

Dr. Duncan J. Hodkinson
Division of Clinical Neuroscience
Sir Peter Mansfield Imaging Centre
Queen's Medical Centre
West Block/ B Floor/ Room W/B1437
University of Nottingham
Nottingham, NG7 2UH, UK
duncan.hodkinson@nottingham.ac.uk
Tel: +44(0)7376916940

Dr. JeYoung Jung
School of Psychology
University of Nottingham
Nottingham, NG7 2RD, UK
Jeyoung.Jung@nottingham.ac.uk
Tel: +44(0)1158467241

Number of pages: 27

Number of figures: 7

Number of tables: 0

ABSTRACT

The ability to induce neuroplasticity with non-invasive brain stimulation techniques offers a unique opportunity to examine the human brain systems involved in pain modulation. In experimental and clinical settings, the primary motor cortex (M1) is commonly targeted to alleviate pain, but its mechanism of action remains unclear. Using dynamic causal modelling (DCM) and Bayesian model selection (BMS), we tested seven competing hypotheses about how TMS modulates the directed influences (or effective connectivity) between M1 and three distinct cortical areas of the medial and lateral pain systems, including the insular (INS), anterior cingulate cortex (ACC), and parietal operculum (PO). The dataset included a novel fMRI acquisition collected synchronously with M1 stimulation during rest and while performing a simple hand motor task. DCM and BMS showed a clear preference for the fully connected model in which all cortical areas receive input directly from M1, with facilitation of the connections INS→M1, PO→M1, and ACC→M1, plus increased inhibition of their reciprocal connections. An additional DCM analysis comparing the reduced models only corresponding to networks with a sparser connectivity within the full model, showed that M1 input into the INS is the second-best model of plasticity following TMS manipulations. The results reported here provide a starting point for investigating whether pathway-specific targeting involving M1↔INS improves analgesic response beyond conventional targeting. We eagerly await future empirical data and models that tests this hypothesis.

NEW & NOTEWORTHY

Transcranial magnetic stimulation of the motor cortex (M1) is a promising treatment for chronic pain, but its mechanism of action remains unclear. Competing dynamic causal models of effective connectivity between M1 and medial and lateral pain systems, suggests direct input into the insular, anterior cingulate cortex, and parietal operculum. This supports the hypothesis that analgesia produced from M1 stimulation most likely acts through the activation of top-down processes associated with intracortical modulation.

INTRODUCTION

Stimulation of the primary motor cortex (M1) by transcranial magnetic stimulation (TMS) has been shown to alleviate pain (Lefaucheur et al. 2014; Mylius et al. 2012). The mechanisms by which TMS exerts these analgesic effects is still unclear. However, there is compelling evidence that TMS can alter cortical excitability via changes in synaptic plasticity through long-term potentiation (LTP) and long-term depression (LDP)-like mechanisms (Thickbroom 2007; Ziemann et al. 2008). These same transduction mechanisms are essential for the development and maintenance of pain hypersensitivity (Ji et al. 2003; Sandkuhler 2007; Woolf and Salter 2000), thus providing a strong rationale for TMS-based therapies in the relief of chronic pain (Ridding and Rothwell 2007).

Relatively little is known about the molecular mechanisms underlying the induction and expression of cortical plasticity following TMS in humans (Ridding and Ziemann 2010). Experimental evidence suggests that TMS modulates a mixture of neuronal populations that use different neurotransmitters, each with a different sensitivity to the stimulation (Hamada et al. 2013). A large body of evidence has also demonstrated that TMS has the capacity to modulate large-scale neural network dynamics across multiple spatial and temporal scales (Dayan et al. 2013; Karabanov et al. 2015; Ozdemir et al. 2020). While this may be only indirect evidence, it demonstrates that brain networks might be used to understand how TMS works and to improve therapy by identifying the best places to stimulate the brain (Fox et al. 2012).

Stimulation of M1 following TMS has been shown to modulate motor brain areas that can influence susceptibility of the corticomotor network (Bestmann et al. 2003; Cardenas-Morales et al. 2014; Munchau et al. 2002), as well as functionally connected non-motor areas such as the insular, operculum, cingulate cortex, auditory gyrus, frontal, and parietal cortex (Bohning et al., 1999, 2000a,b, Baudewig et al, 2001, Bestmann et al, 2003, Denslow et al., 2005, Jung et al., 2016). We recently demonstrated that short-trains of 1Hz TMS pulses over M1 can induce increased activation in the bilateral insular and opercular cortex (Jung et al., 2016, 2020). Similarly, Cocchi *et al* (2015) reported that continuous theta burst stimulation (cTBS) over the M1 not only activated the insular and operculum but also increased functional connectivity between the two regions (Cocchi et al. 2015). These findings suggest that intracortical connections

between M1 and operculo-insular cortex may be a modifiable pathway for plasticity following TMS manipulations.

Recent targeted applications of TMS have been guided by differences in intrinsic functional connectivity (FC) rather than brain anatomy (Weigand et al. 2018). The combination of TMS with FC mapping is particularly well suited to study changes in brain networks (Hampson and Hoffman 2010; Paus 2005). Local stimulation to an accessible network node can propagate (trans-synaptically) to distal but interconnected nodes with high spatial specificity (Bestmann et al. 2005; Ruff et al. 2008). This coupling allows for causality to be inferred between the applied stimulation site and the observed changes in network connectivity (Friston 2011). Furthermore, prospective mechanistic and interpretative models of brain function can be used to provide estimates of the effective strength of synaptic connections and their context-dependent modulation (Polania et al. 2018; Zanto et al. 2011).

Dynamic causal modelling (DCM) is the most widely used method for inferring effective connectivity within networks of distributed neuronal responses (Daunizeau et al. 2011; Friston et al. 2003). This technique has been used in the analysis of a wide range of neuroimaging (Friston et al. 2003) and electrophysiology data (David et al. 2006) to test competing hypotheses about the neuronal states underlying experimental measurements of human brain activity. DCM is considered most appropriate for explaining brain responses induced by experimental interventions that cause fast changes in neuronal excitability and/or connection strength. In this context, the combination of DCM

and fMRI has been applied to study specific aspects of human pain processing (Liang et al. 2013; 2011) and descending modulation (Sevel et al. 2015a; Sevel et al. 2015b). However, its applications into the neurophysiology of non-invasive brain stimulation techniques for pain control remains limited.

Here we used DCM and Bayesian model selection (BMS) to examine how TMS modulates the directed influences (or effective connectivity) between M1 and three distinct cortical areas of the medial and lateral pain systems, including the insular (INS), anterior cingulate (ACC), and parietal operculum (PO, the secondary somatosensory cortex). As these structures have specific reciprocal interconnections (Eickhoff et al. 2010; Ghaziri et al. 2017), we allowed for a fully connected model and reduced models corresponding to networks with a sparser connectivity contained within this larger model. This resulted in seven possible pathways through which M1 stimulation could influence the proposed system: 1) ACC and PO receive input directly from M1; 2) INS and PO receive input directly from M1; 3) ACC and INS receive input directly from M1; 4) ACC receives input directly from M1; 5) PO receives input directly from M1; 6) INS receives input directly from M1, and 7) ACC, INS, PO collectively receives input directly from M1 (fully-connected model). The dataset used to test these competing hypotheses included a novel fMRI acquisition collected synchronously with M1 stimulation during rest and while performing a simple hand motor task (Jung et al. 2020). We expected that DCM and BMS would show the plausibility of alternative neurophysiological explanations for the analgesic effects of M1 stimulation.

MATERIALS & METHODS

Ethics statement

This study was approved by the local research ethics committee at the University of Nottingham and performed in accordance with Declaration of Helsinki. All participants provided informed written consent prior to the experiment.

Study participants

Twenty-three healthy, right-handed adults (6 males, mean age = 26 ± 3 years, range 19–32 years) participated in the study. The data was from a previously published study (Jung et al. 2020) involving M1 stimulation with TMS under resting conditions. This cohort included a subgroup of participants that also performed a motor task during M1 stimulation (task group: *N*=12, 3 males, mean age 27 ± 3 years, range 20–32 years).

TMS and synchronized TMS/fMRI

A Magstim Rapid2 stimulator (Magstim, UK) was used to generate TMS pulses through an MR-compatible figure-of-eight coil (70mm). Individual resting motor threshold (RMT) was measured outside of the scanner before the experiment. Individual RMTs were measured as follows: TMS pulses were applied to the M1 to identify the optimal site eliciting a muscle twitch in the first dorsal interosseous

(FDI) muscle and the TMS coil was oriented perpendicular to the central sulcus at a 45° angle from the mid-sagittal line approximately. Once a site was identified, the stimulator intensity was systematically varied and the RMT was defined as the minimum stimulator output that was required to induce an observable muscle twitch at that site for five out of 10 TMS pulses. During the scanning, the coil was position over the hotspot of right hand area in the left hemisphere. Individual TMS intensity was 100% of RMT for the M1 stimulation. The averaged RMT was 75% in the task M1 stimulation group (range 64–89%) and 72% in the rest group, the mean (range 59% to 86%).

TMS pulse was synchronized with the fMRI acquisition as described previously (Jung et al. 2016) (see Figure 1A). The scanner sequence was programmed to split the acquisition of images in each volume into two separate packages. The first package was acquired for ~800ms and the second package commenced collection 200ms after the first package acquisition. A TMS pulse was applied at 850ms and 1,850ms after the acquisition of the first slice in each package during the TMS phase.

Experimental design and procedures

A block-design fMRI paradigm was used with nine separate blocks (block length of 30s) (Figure 1B). Each block consisted of an active TMS phase (11s) and inactive TMS phase (19s). The onset of TMS was randomized within a block. For the active TMS phase, 11 pulses of 1Hz TMS was delivered over the left motor cortex during rest and while performing a simple hand motor task. The instruction

to participants was to continuously clench and unclench their hands with a rate that they were comfortable with (around 0.5~1Hz). The task cues presented on the screen were “left hand”, “right hand”, “both hands”, and “rest”. The order of the task conditions was pseudorandomised. For the rest condition, participants were asked to relax and view a fixation on the screen during the scanning.

MRI acquisition

A 3T Philips Achieva scanner was used to collect data with a 6-channel NOVA head coil that accommodated the MR-compatible TMS coil. Functional images were acquired using single-shot echo-planar imaging (EPI) sequence [TR/TE=2000/35ms, 30 slices=30, resolution=3×3×3 mm^3, FA=90°]. Structural image was obtained using 3D MP-RAGE sequence [TR/TE = 8.278/2.3ms, resolution=1×1×1mm^3, FA=8°) covering the whole head. The TMS-coil was MR-visible for short echo-time (TE<10ms) and was used to verify the position of the TMS-coil relative to the subject. Target sites for stimulation were defined as the point on the brain surface perpendicular to the centre of the TMS coil (where the two rings of the figure-of-eight meet each other). This position was translated into MNI space (see Figure 1C and Table S1).

Image processing and GLM analysis

All imaging data were preprocessed and analyzed using SPM12 (https://www.fil.ion.ucl.ac.uk/spm/software/spm12/) (for details see (Jung et al. 2020)). Pre-processing included spatial realignment, co-registration of each

individual's mean functional image to their anatomical imaging, spatial normalization and smoothing using a Gaussian kernel (8 mm, Full-width half-maximal). A general linear model (GLM) was used to compute individual contrasts. For the task group, a design matrix was defined with four task conditions (rest, left, right, and both hand clenching) and TMS phases (TMS vs no-TMS). T-contrasts for each condition and TMS phase were established. In the random effect analysis, two-factorial ANOVA with the task condition and TMS (active vs. inactive) was conducted and contrasts were entered into a set of one-sample t-tests for each condition. Head movement parameters were included as regressors to exclude head movement-related variance. For the rest condition, a design matrix with TMS phases (active and inactive) was constructed. In the random effect analysis, the contrast images were entered into one-sample t-tests (Figure 2A/B). The statistical significance threshold was at $p < 0.005$ at the voxel level with false-discovery rate (FDR) correction for a cluster level, $p < 0.05$, $Ks > 50$.

Psychophysiological interaction (PPI)

We performed a psychophysiological interaction (PPI) analysis (Friston et al. 1997) of the functional connectivity in M1 (Figure 2C). The M1 ROI was defined as the left M1 [MNI -33, -24, 63] from the GLM results as a seed region. From this seed region (8mm sphere), the time courses were de-convolved based on the model for the canonical hemodynamic response to construct a time series of neural activity. Interaction terms were calculated separately for the TMS active

and inactive conditions, as the product between the vector of the condition and the psychological factor. The PPI terms were also been convolved with the hemodynamic response function. The preprocessed fMRI data was entered into the CONN toolbox (Whitfield-Gabrieli and Nieto-Castanon 2012) for the PPI analysis. Data were filtered using a band pass filter ($0.01 < f < 2$) to decrease the effect of low-frequency drift. White matter, cerebrospinal fluid, and physiological noise source reduction were taken as confounds, following the implemented CompCor strategy (Behzadi et al. 2007). Head motion was taken into account and rotational and translational motion parameters and their first-order temporal derivatives were regressed out. The onset and duration of each experimental condition was supplied to the toolbox. For group-level analysis, individual results were converted to z-scores with Fisher's z-transformation. As the PPI is very stringent (O'Reilly et al. 2012), we used the significance threshold at $p < 0.01$ uncorrected, $Ks > 50$.

Dynamic Causal Modelling

Based on the results of PPI, we next used DCM to investigate how TMS modulates the directed influences (or effective connectivity) between M1 and the cortical areas defined above. DCM is a method for estimating and making inferences about coupling among brain regions and provides information about the underlying cortical pathways and their causal relationships (Friston et al. 2003). DCM estimates task-independent "intrinsic" connectivity, the "modulatory" changes in the connectivity induced by a specific task (e.g., TMS and hand

clenching task), and the extrinsic influence of “inputs” on regions (i.e. the driving input). We constructed DCM models that represented all possible configurations of the modulatory parameters between M1 and the cortical areas of the medial and lateral pain systems, including the insular (INS), anterior cingulate (ACC), and parietal operculum (PO, the secondary somatosensory cortex). As these structures have specific reciprocal interconnections (Eickhoff et al. 2010; Ghaziri et al. 2017), we allowed for a fully connected model and reduced models corresponding to networks with a sparser connectivity contained within this larger model. This resulted in seven possible pathways through which M1 stimulation could influence the proposed system: 1) ACC and PO receive input directly from M1; 2) INS and PO receive input directly from M1; 3) ACC and INS receive input directly from M1; 4) ACC receives input directly from M1; 5) PO receives input directly from M1; 6) INS receives input directly from M1, and 7) ACC, INS, PO collectively receive input directly from M1 (fully-connected model) (Figure 3). The M1 TMS was entered as a driving input to the models. For the DCM analysis, we extracted the first eigenvariate (devolved neural activity) from a spherical ROI (radius = 8mm) centered at the maximally responsive point of the left M1 defined *a priori* by the main effect of the motor task in the GLM analysis. The INS [MNI -36, 12, 10], PO [MNI -44, -6, 6], and ACC [MNI -6, -18, 30] were defined *a priori* by the PPI analysis. We restricted our model within the left hemisphere as TMS was applied over the left M1.

Bayesian model selection

The seven competing models were compared using Bayesian model selection (BMS) (Penny et al. 2004; Stephan et al. 2009) to determine the model which provides the best fit between accuracy and generalizability in the given fMRI data. In the resting condition, TMS phases were modelled as experimental perturbations for all subjects (*N*=23). However, in the task subgroup (N=12), both task conditions (left, right, and both hand clenching) and TMS phases (active and inactive) were modelled as experimental perturbations of the system. Then DCMs of the wining model were estimated separately for each participant, allowing an identification of changes in interregional connectivity induced by the M1 TMS. The estimated intrinsic and modulatory connections were considered significant when passing a threshold of $p_{FDR\text{-}corrected} < 0.05$ (one-sample tests). In order to identify connections specifically modulated by TMS, we compared modulatory connectivity between the TMS active and inactive conditions (planned paired tests, $p < 0.05$).

RESULTS

ROI selection

A detailed description of the fMRI analysis has been published previously (Jung et al. 2020). Main effects of the hand clenching motor task and local activation maxima for the hand somatotopic region within M1 are shown in Figure 2A. The results showed a significant main effect in the bilateral M1, premotor cortex, and

supplementary motor area. Conjunction analysis of the M1 stimulation in active TMS compared to inactive TMS phases is shown in Figure 2B. Stimulation in M1 resulted in significant activation of the insula, inferior frontal gyrus (IFG) and PO. We hypothesized that the functional connectivity between M1 and three independent brain areas – insular (INS), anterior cingulate (ACC), and secondary somatosensory cortex (PO) – may reflect a susceptibility for plasticity following TMS manipulation. Thus, we performed a psychophysiological interaction (PPI) analysis (Friston et al. 1997) of the functional connectivity in M1. The PPI analysis with the M1 seed revealed that active-TMS over the M1 strengthened connectivity with several brain areas (including the INS, ACC and PO) relative to the inactive TMS phase (Figure 2C and Table S2). The result confirm that the functional state and connectivity profile of the three *a priori* brain areas appears to reflect the individual's susceptibility to TMS manipulation.

DCM and BMS: model estimation and selection

The next question was to explore what drives the individual's connectivity profile. The results of the BMS with expected and exceedance probabilities using random effects (RFX) analysis are shown in Figure 4A. Under resting conditions (resting group, *N*=23), Model 7 was the model with the highest exceedance probability thus the winning network model. Using the best model (model 7), we further compared the modulatory connectivity between active and inactive TMS conditions between the distinct brain areas (Figure 4B). The paired t-tests demonstrated that active TMS significantly increased effective connectivity from

ACC→M1 (t = -2.16, p = 0.042), INS→M1 (t = -2.21, p = 0.046), and PO→M1 (t = -2.22, p = 0.046) in comparison to inactive TMS phase. In contrast, there was a decrease in effective connectivity from M1→INS (t = 2.52, p = 0.020) and M1→ACC (t = 2.19, p = 0.04). The driving inhibitory input to M1 by TMS was also significant (t= -2.15, p = 0.043). It should be noted that there was no significant intrinsic connection between the ROIs. A full list of parameter estimates is available in Table S3.

We also conducted the same analysis under task conditions (task group, *N*=12). The BMS results demonstrated that the winning model was model 7, replicating the whole group results (Figure 5A). The results of rest condition revealed that active TMS significantly increased effective connectivity from ACC→M1 (Z = -2.51, p = 0.012), INS→M1 (Z = -2.19, p = 0.030), and PO→M1 (Z = -2.20, p = 0.028), whereas decreased effective connectivity from the M1 to ACC (Z = -1.96, p = 0.05) and to insular (Z = -2.89, p = 0.041) during active TMS (Figure 5B and Table S4). DCM parameter estimates during each task condition are shown in Figure 5C. As previously described (Jung et al. 2020), the motor task reduced the INS and PO activation related to the M1 TMS. We did not find any significant difference between the active and inactive TMS phase when the left hemisphere was engaged in the task (right and both hand clenching). However, M1 TMS evoked a significant decreased connectivity from the INS to M1 during the left hand clenching only (Z = -2.28, p = 0.023) (Figure 5C and Table S5). The driving input, M1 TMS was significant at rest (p = 0.0009), left hand (p = 0.019), right hand (p = 0.005), and both hand conditions (p = 0.005).

In an additional DCM analysis, we examined more closely the difference between the winning model and the second-best model (model 6). The 'best' model can depend critically on which set of models are being compared, and it is possible that augmenting the comparison set with a single extra model could alter the ranking of the models (Penny et al. 2010). We performed an additional analysis comparing the reduced models only (models 1-6) corresponding to networks with a sparser connectivity within the full model. We found that Model 6 remains the dominant reduced model under resting conditions (resting group, *N*=23) (Figure 6). The paired t-tests demonstrated that active TMS significantly increased effective connectivity from INS→M1 t = -2.11, p = 0.046) and ACC→PO (t = -2.25, p = 0.035) in comparison to inactive TMS phase. In contrast, there was a decrease in effective connectivity from M1→INS (t = 2.54, p = 0.019). The driving inhibitory input to M1 by TMS was also significant (*t*=-2.394, *p* = 0.026). A full list of parameter estimates is available in Table S6.

We also conducted the same analysis under task conditions (task group, *N*=12). The BMS results demonstrated that the winning model was again model 6, replicating the whole group results (Figure 7A). The results of rest condition revealed that active TMS significantly increased effective connectivity from INS→M1 (Z = -2.20, p = 0.028) and from ACC→PO (Z = -2.47, p = 0.013), whereas decreased effective connectivity from the M1 to insular (Z = -1.89, p = 0.059) during active TMS (Figure 7B). One-sample Wiscoxon Signed Rank tests demonstrated significant facilitatory connections from ACC→PO, ACC→INS, PO→INS, and INS→M1 as well as a significant inhibitory connection from

M1→INS (ps $_{FDR\text{-}corrected}$ < 0.05) (Table S7). DCM parameter estimates during each task condition are shown in Figure 7C. We did not find any significant difference between the active and inactive TMS phase when the left hemisphere was engaged in the task (right and both hand clenching). However, M1 TMS evoked a significant decreased connectivity from the INS to M1 during the left hand clenching only (Z = -2.35, p = 0.019) (Figure 7C and Table S8). The driving input, M1 TMS was significant at rest (p = 0.039), left hand (p = 0.012), and both hand conditions (p = 0.004). Altogether, this corroborated the results from the initial model selection procedure that model 6 represents the second-best model following the fully connected network.

Supplemental material is available at:

https://figshare.com/search?q=JN_2021_Hodkinson_SupplementalMaterial

DISCUSSION

Using DCM and BMS, we tested seven competing hypotheses about how TMS modulates the directed influences (or effective connectivity) between M1 and three distinct cortical areas of the medial and lateral pain systems, including the insular (INS), anterior cingulate (ACC), and parietal operculum (PO). The dataset included a novel fMRI acquisition collected synchronously with M1 stimulation during rest and while performing a simple hand motor task (Jung et al. 2020). DCM and BMS showed a clear preference for the fully connected model in which

M1 stimulation causally determines activity in the INS, PO, and ACC under resting conditions. In the following discussion, we consider the potential mechanisms underlying TMS-induced changes in cortical plasticity and its relevance to pain control.

The rationale for applying TMS to treat pain is that it can induce long-lasting, and potentially reversible therapeutic changes in cortical plasticity. Our results confirmed that TMS stimulation has a rapid effect on cortical excitability, which extends beyond the local stimulated area. The excitation of the connections INS→M1, PO→M1, and ACC→M1, plus the increased inhibition of their reciprocal connections, suggests that these structures are tightly and probably bidirectionally coupled. This supports the hypothesis that analgesia produced from M1 stimulation most likely acts through the activation of top-down processes associated with intracortical modulation, and not spinal inhibition via direct stimulation of the pyramidal tract (Nguyen et al. 2011). Whilst the driving input to M1 by TMS was shown to be inhibitory, the stimulation of the fibers running parallel to the cortical surface in the precentral gyrus could lead to both orthodromic activation of corticofugal pathways as well as antidromic activation of thalamocortical pathways (Tranchina and Nicholson 1986). Further studies are required to dissect these interareal connections at finer levels, and to link TMS response properties of neurons in these different subregions to specific sensory modalities. Nevertheless, it could account for the influence on pathways and structures that are distant from the site of stimulation.

The reduced models of network connectivity and their observed responses to TMS have the potential to expand our knowledge of pain control and in evaluating the therapeutic potential of TMS. We observed that M1 input into the INS represents the second-best model of plasticity following TMS manipulations. INS and the adjacent PO are the only cortical brain regions that can trigger a painful percept when electrically stimulated (Afif et al. 2008; Mazzola et al. 2012; Ostrowsky et al. 2000). Whilst activation of the postero-superior insula triggers pain and thermal sensations, inhibition of the same region can potentially induce analgesia and loss of thermal sensation. For example, ischaemic lesions restricted to the postero-superior operculo-insular region can impair discrimination of thermal sensations by increasing the thermal pain threshold detection (Garcia-Larrea et al. 2010; Greenspan et al. 1999; Veldhuijzen et al. 2010). Interestingly, Lenoir et al. (2018) recently demonstrated a modulatory effect of continuous theta-burst stimulation (cTBS) over the human operculo-insular cortex using a coil designed for deep TMS. They showed that cTBS selectively affects the perception of heat pain without any changes to the perception of cold, warm or vibrotactile stimuli (Lenoir et al. 2018). These findings speak to the potential advantages of non-invasive stimulation of the INS to produce analgesia; however, the authors also reported that cTBS delivered over that structure is associated with a higher risk of triggering a TMS-induced seizure. We speculate that it may be possible to impart equivalent symptomatic benefit without the seizure risk through targeting M1 sites that are more

functionally connected to the INS; however this remains a hypothesis and requires formal testing.

There are several limitations and interesting questions raised by the current study that should be addressed. Firstly, it remains unclear how long the aftereffects from TMS can last, and whether the reversal rate depends on the duration of TMS stimulation. In the current experiment, we employed repeated pulses at 1Hz that was similar in duration to conventional rTMS protocols and resulted in an inhibitory effect on M1 in the healthy subjects. However, development of clinically relevant dosing parameters related to the cumulative exposure of TMS needs systematic evaluation. The method of the fMRI data collection should also be considered, as the current work leverages a unique dataset in which the TMS pulse was synchronised to be delivered with fMRI acquisition (Jung et al. 2016). This resource has yielded some of the most informative results to date showing a rapid effect on cortical excitability. Likewise, the DCM and BMS analysis provided a powerful tool for testing hypothesis related to the directional connections most susceptible to TMS manipulation. Unfortunately, due to the lack of an explicit nociceptive stimulus, the specificity of the selected brain areas cannot be interpreted as pain responsive, thus any classification of brain circuitry using such areas should be interpreted with caution. Finally, it remains unclear which part of the human M1 should be stimulated, and which downstream regions are important for analgesic efficacy. The selective reconfiguration of the INS delineated by the DCM analysis may be a substrate for plasticity following TMS manipulations. The results reported here

provide a starting point for investigating whether pathway-specific targeting involving M1↔INS improves analgesic response beyond conventional targeting. We eagerly await future empirical data and models that tests this hypothesis.

ACKNOWLEDGMENTS

DJH would like to thank John N. Hodkinson for reviewing the manuscript and Dorothee Auer for advice and guidance relating to this work.

CONFLICT OF INTEREST

The authors declare no conflict of interest with regard to the content of this article.

FUNDING SOURCES

DJH is supported by funding from the NIHR Nottingham BRC.

REFERENCES

Afif A, Hoffmann D, Minotti L, Benabid AL, and Kahane P. Middle short gyrus of the insula implicated in pain processing. *Pain* 138: 546-555, 2008.

Behzadi Y, Restom K, Liau J, and Liu TT. A component based noise correction method (CompCor) for BOLD and perfusion based fMRI. *Neuroimage* 37: 90-101, 2007.

Bestmann S, Baudewig J, Siebner HR, Rothwell JC, and Frahm J. BOLD MRI responses to repetitive TMS over human dorsal premotor cortex. *Neuroimage* 28: 22-29, 2005.

Bestmann S, Baudewig J, Siebner HR, Rothwell JC, and Frahm J. Subthreshold high-frequency TMS of human primary motor cortex modulates

interconnected frontal motor areas as detected by interleaved fMRI-TMS. *Neuroimage* 20: 1685-1696, 2003.

Cardenas-Morales L, Volz LJ, Michely J, Rehme AK, Pool EM, Nettekoven C, Eickhoff SB, Fink GR, and Grefkes C. Network connectivity and individual responses to brain stimulation in the human motor system. *Cereb Cortex* 24: 1697-1707, 2014.

Cocchi L, Sale MV, Lord A, Zalesky A, Breakspear M, and Mattingley JB. Dissociable effects of local inhibitory and excitatory theta-burst stimulation on large-scale brain dynamics. *J Neurophysiol* 113: 3375-3385, 2015.

Daunizeau J, David O, and Stephan KE. Dynamic causal modelling: a critical review of the biophysical and statistical foundations. *Neuroimage* 58: 312-322, 2011.

David O, Kiebel SJ, Harrison LM, Mattout J, Kilner JM, and Friston KJ. Dynamic causal modeling of evoked responses in EEG and MEG. *Neuroimage* 30: 1255-1272, 2006.

Dayan E, Censor N, Buch ER, Sandrini M, and Cohen LG. Noninvasive brain stimulation: from physiology to network dynamics and back. *Nat Neurosci* 16: 838-844, 2013.

Eickhoff SB, Jbabdi S, Caspers S, Laird AR, Fox PT, Zilles K, and Behrens TE. Anatomical and functional connectivity of cytoarchitectonic areas within the human parietal operculum. *J Neurosci* 30: 6409-6421, 2010.

Fox MD, Halko MA, Eldaief MC, and Pascual-Leone A. Measuring and manipulating brain connectivity with resting state functional connectivity magnetic resonance imaging (fcMRI) and transcranial magnetic stimulation (TMS). *Neuroimage* 62: 2232-2243, 2012.

Friston KJ. Functional and effective connectivity: a review. *Brain Connect* 1: 13-36, 2011.

Friston KJ, Buechel C, Fink GR, Morris J, Rolls E, and Dolan RJ. Psychophysiological and modulatory interactions in neuroimaging. *Neuroimage* 6: 218-229, 1997.

Friston KJ, Harrison L, and Penny W. Dynamic causal modelling. *Neuroimage* 19: 1273-1302, 2003.

Garcia-Larrea L, Perchet C, Creac'h C, Convers P, Peyron R, Laurent B, Mauguiere F, and Magnin M. Operculo-insular pain (parasylvian pain): a distinct central pain syndrome. *Brain* 133: 2528-2539, 2010.

Ghaziri J, Tucholka A, Girard G, Houde JC, Boucher O, Gilbert G, Descoteaux M, Lippe S, Rainville P, and Nguyen DK. The Corticocortical Structural Connectivity of the Human Insula. *Cereb Cortex* 27: 1216-1228, 2017.

Greenspan JD, Lee RR, and Lenz FA. Pain sensitivity alterations as a function of lesion location in the parasylvian cortex. *Pain* 81: 273-282, 1999.

Hamada M, Murase N, Hasan A, Balaratnam M, and Rothwell JC. The role of interneuron networks in driving human motor cortical plasticity. *Cereb Cortex* 23: 1593-1605, 2013.

Hampson M, and Hoffman RE. Transcranial magnetic stimulation and connectivity mapping: tools for studying the neural bases of brain disorders. *Front Syst Neurosci* 4: 2010.

Ji RR, Kohno T, Moore KA, and Woolf CJ. Central sensitization and LTP: do pain and memory share similar mechanisms? *Trends Neurosci* 26: 696-705, 2003.

Jung J, Bungert A, Bowtell R, and Jackson SR. Modulating Brain Networks With Transcranial Magnetic Stimulation Over the Primary Motor Cortex: A Concurrent TMS/fMRI Study. *Front Hum Neurosci* 14: 31, 2020.

Jung J, Bungert A, Bowtell R, and Jackson SR. Vertex Stimulation as a Control Site for Transcranial Magnetic Stimulation: A Concurrent TMS/fMRI Study. *Brain Stimul* 9: 58-64, 2016.

Karabanov A, Ziemann U, Hamada M, George MS, Quartarone A, Classen J, Massimini M, Rothwell J, and Siebner HR. Consensus Paper: Probing Homeostatic Plasticity of Human Cortex With Non-invasive Transcranial Brain Stimulation. *Brain Stimul* 8: 442-454, 2015.

Lefaucheur JP, Andre-Obadia N, Antal A, Ayache SS, Baeken C, Benninger DH, Cantello RM, Cincotta M, de Carvalho M, De Ridder D, Devanne H, Di Lazzaro V, Filipovic SR, Hummel FC, Jaaskelainen SK, Kimiskidis VK, Koch G, Langguth B, Nyffeler T, Oliviero A, Padberg F, Poulet E, Rossi S, Rossini PM, Rothwell JC, Schonfeldt-Lecuona C, Siebner HR, Slotema CW, Stagg CJ, Valls-Sole J, Ziemann U, Paulus W, and Garcia-Larrea L. Evidence-based guidelines on the therapeutic use of repetitive transcranial magnetic stimulation (rTMS). *Clin Neurophysiol* 125: 2150-2206, 2014.

Lenoir C, Algoet M, and Mouraux A. Deep continuous theta burst stimulation of the operculo-insular cortex selectively affects Adelta-fibre heat pain. *J Physiol* 596: 4767-4787, 2018.

Liang M, Mouraux A, and Iannetti GD. Bypassing primary sensory cortices--a direct thalamocortical pathway for transmitting salient sensory information. *Cereb Cortex* 23: 1-11, 2013.

Liang M, Mouraux A, and Iannetti GD. Parallel processing of nociceptive and non-nociceptive somatosensory information in the human primary and secondary somatosensory cortices: evidence from dynamic causal modeling of functional magnetic resonance imaging data. *J Neurosci* 31: 8976-8985, 2011.

Mazzola L, Isnard J, Peyron R, and Mauguiere F. Stimulation of the human cortex and the experience of pain: Wilder Penfield's observations revisited. *Brain* 135: 631-640, 2012.

Munchau A, Bloem BR, Irlbacher K, Trimble MR, and Rothwell JC. Functional connectivity of human premotor and motor cortex explored with repetitive transcranial magnetic stimulation. *J Neurosci* 22: 554-561, 2002.

Mylius V, Borckardt JJ, and Lefaucheur JP. Noninvasive cortical modulation of experimental pain. *Pain* 153: 1350-1363, 2012.

Nguyen JP, Nizard J, Keravel Y, and Lefaucheur JP. Invasive brain stimulation for the treatment of neuropathic pain. *Nat Rev Neurol* 7: 699-709, 2011.

O'Reilly JX, Woolrich MW, Behrens TE, Smith SM, and Johansen-Berg H. Tools of the trade: psychophysiological interactions and functional connectivity. *Soc Cogn Affect Neurosci* 7: 604-609, 2012.

Ostrowsky K, Isnard J, Ryvlin P, Guenot M, Fischer C, and Mauguiere F. Functional mapping of the insular cortex: clinical implication in temporal lobe epilepsy. *Epilepsia* 41: 681-686, 2000.

Ozdemir RA, Tadayon E, Boucher P, Momi D, Karakhanyan KA, Fox MD, Halko MA, Pascual-Leone A, Shafi MM, and Santarnecchi E. Individualized perturbation of the human connectome reveals reproducible biomarkers of network dynamics relevant to cognition. *Proc Natl Acad Sci U S A* 117: 8115-8125, 2020.

Paus T. Inferring causality in brain images: a perturbation approach. *Philos Trans R Soc Lond B Biol Sci* 360: 1109-1114, 2005.

Penny WD, Stephan KE, Daunizeau J, Rosa MJ, Friston KJ, Schofield TM, and Leff AP. Comparing families of dynamic causal models. *PLoS Comput Biol* 6: e1000709, 2010.

Penny WD, Stephan KE, Mechelli A, and Friston KJ. Modelling functional integration: a comparison of structural equation and dynamic causal models. *Neuroimage* 23 Suppl 1: S264-274, 2004.

Polania R, Nitsche MA, and Ruff CC. Studying and modifying brain function with non-invasive brain stimulation. *Nat Neurosci* 21: 174-187, 2018.

Ridding MC, and Rothwell JC. Is there a future for therapeutic use of transcranial magnetic stimulation? *Nat Rev Neurosci* 8: 559-567, 2007.

Ridding MC, and Ziemann U. Determinants of the induction of cortical plasticity by non-invasive brain stimulation in healthy subjects. *J Physiol* 588: 2291-2304, 2010.

Ruff CC, Bestmann S, Blankenburg F, Bjoertomt O, Josephs O, Weiskopf N, Deichmann R, and Driver J. Distinct causal influences of parietal versus frontal areas on human visual cortex: evidence from concurrent TMS-fMRI. *Cereb Cortex* 18: 817-827, 2008.

Sandkuhler J. Understanding LTP in pain pathways. *Mol Pain* 3: 9, 2007.

Sevel LS, Craggs JG, Price DD, Staud R, and Robinson ME. Placebo analgesia enhances descending pain-related effective connectivity: a dynamic causal modeling study of endogenous pain modulation. *J Pain* 16: 760-768, 2015a.

Sevel LS, O'Shea AM, Letzen JE, Craggs JG, Price DD, and Robinson ME. Effective connectivity predicts future placebo analgesic response: A dynamic causal modeling study of pain processing in healthy controls. *Neuroimage* 110: 87-94, 2015b.

Stephan KE, Penny WD, Daunizeau J, Moran RJ, and Friston KJ. Bayesian model selection for group studies. *Neuroimage* 46: 1004-1017, 2009.

Thickbroom GW. Transcranial magnetic stimulation and synaptic plasticity: experimental framework and human models. *Exp Brain Res* 180: 583-593, 2007.

Tranchina D, and Nicholson C. A model for the polarization of neurons by extrinsically applied electric fields. *Biophys J* 50: 1139-1156, 1986.

Veldhuijzen DS, Greenspan JD, Kim JH, and Lenz FA. Altered pain and thermal sensation in subjects with isolated parietal and insular cortical lesions. *Eur J Pain* 14: 535 e531-511, 2010.

Weigand A, Horn A, Caballero R, Cooke D, Stern AP, Taylor SF, Press D, Pascual-Leone A, and Fox MD. Prospective Validation That Subgenual Connectivity Predicts Antidepressant Efficacy of Transcranial Magnetic Stimulation Sites. *Biol Psychiatry* 84: 28-37, 2018.

Whitfield-Gabrieli S, and Nieto-Castanon A. Conn: a functional connectivity toolbox for correlated and anticorrelated brain networks. *Brain Connect* 2: 125-141, 2012.

Woolf CJ, and Salter MW. Neuronal plasticity: increasing the gain in pain. *Science* 288: 1765-1769, 2000.

Zanto TP, Rubens MT, Thangavel A, and Gazzaley A. Causal role of the prefrontal cortex in top-down modulation of visual processing and working memory. *Nat Neurosci* 14: 656-661, 2011.

Ziemann U, Paulus W, Nitsche MA, Pascual-Leone A, Byblow WD, Berardelli A, Siebner HR, Classen J, Cohen LG, and Rothwell JC. Consensus: Motor cortex plasticity protocols. *Brain Stimul* 1: 164-182, 2008.

FIGURES & LEGENDS

Figure 1: Experimental design and procedures. A) Equipment for the synchronization of TMS/fMRI. **B)** Block design for resting and task M1 stimulation. **(C)** Target sites defined using TMS coil position.

Figure 2. TMS and task interactions. A) GLM results of main effect of motor task (left hand, right hand, and both hands clenching). **(B)** Conjunction analysis (active TMS vs inactive TMS). **(C)** PPI results of the M1 seed revealed active-TMS strengthened connectivity with several brain areas (including the INS, ACC and PO) relative to the inactive TMS phase. To better visualize the INS-PO region we show the results as inflated projections on the PALS-B12 atlas. White rings represent *a priori* regions of interest (ROIs) used for the DCM analysis.

Figure 3. Comparative DCM network models. (A) Full network model with direct input by TMS in the primary motor cortex (M1). The intrinsic connections are indicated by the black lines with arrows, and the arrows indicate the direction of the connectivity **(B)** The six reduced networks (model 1-6) were constructed to represent all possible configurations of the modulatory parameters between M1 and the cortical areas of the medial and lateral pain systems, including the insular (INS), anterior cingulate (ACC), and parietal operculum (PO, the secondary somatosensory cortex). These structures also possessed specific reciprocal interconnections.

Figure 4. Model selection and parameter estimation under resting conditions. (A) The results of Bayesian model selection (BMS) with expected probability and exceedance probability using random effects (RFX) analysis. **(B)** Estimated parameters of the winning network model (Model 7 is the model with the highest exceedance probability). The dotted black arrows represent non-significant connectivity. The black arrows represent the modulatory connections [one-sample t-test, $p_{FDR\text{-}corrected}<0.05$]. The red and blue arrows represent increased and decreased (facilitatory and inhibitory) connectivity during active compared to inactive TMS [paired t-test, $p<0.05$].

Figure 5. DCM parameter estimation under task conditions. (A) The results of Bayesian model selection (BMS) with expected probability and exceedance probability using random effects (RFX) analysis. **(B)** Estimated parameters of the winning network model at rest. **(C)** The estimated parameters for three task conditions: left hand clenching, right hand clenching, and both hand clenching. The dotted black arrows represent non-significant connectivity. The black arrows represent the modulatory connections [one-sample Wilcoxon Signed Ranks test, $p_{FDR\text{-}corrected}<0.05$]. The red and blue arrows represent increased and decreased (facilitatory and inhibitory) connectivity during active compared to inactive TMS.

Figure 6. Reduced model selection and parameter estimation under resting conditions. (A) The results of Bayesian model selection (BMS) with expected probability and exceedance probability using random effects (RFX) analysis. **(B)** Estimated parameters of the winning network model (Model 6 is the model with the highest exceedance probability). The dotted black arrows represent non-significant connectivity. The black arrows represent the modulatory connections [one-sample t-test, $p_{FDR\text{-}corrected}<0.05$]. The red and blue arrows represent increased and decreased (facilitatory and inhibitory) connectivity during active compared to inactive TMS [paired t-test, $p<0.05$].

Figure 7. Reduced model selection and parameter estimation under task conditions. (A) The results of Bayesian model selection (BMS) with expected probability and exceedance probability using random effects (RFX) analysis. **(B)** Estimated parameters of the winning network model at rest. **(C)** The estimated parameters for three task conditions: left hand clenching, right hand clenching, and both hand clenching. The dotted black arrows represent non-significant connectivity. The black arrows represent the modulatory connections [one-sample Wilcoxon Signed Ranks test, $p_{FDR\text{-}corrected}<0.05$]. The red and blue arrows represent increased and decreased (facilitatory and inhibitory) connectivity during active compared to inactive TMS.

A

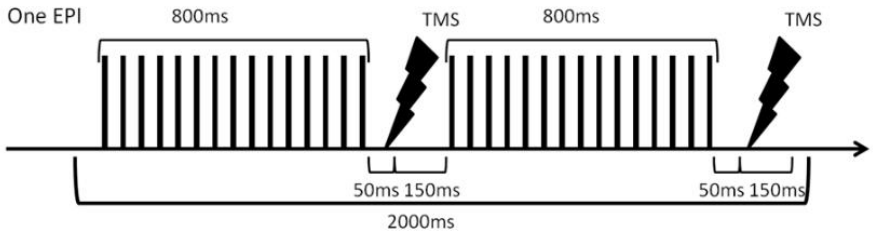
One EPI
800ms
TMS
800ms
TMS
50ms 150ms
50ms 150ms
2000ms

B


Rest
Right
Left
Both
Rest
Both
Right
Left
Rest
1Hz, 11 pulses TMS
30sec

C

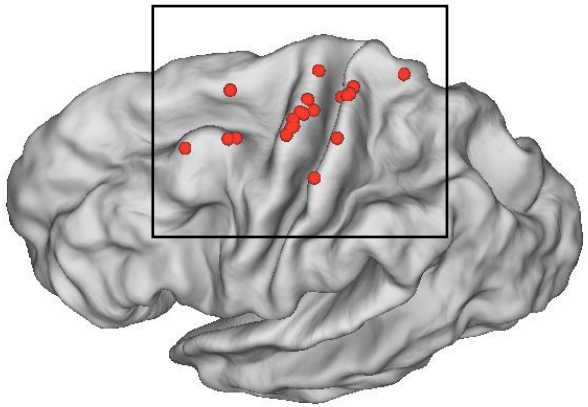

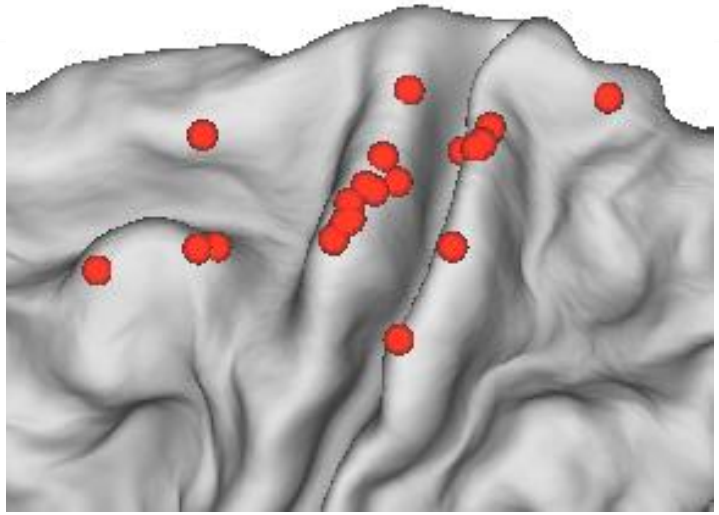

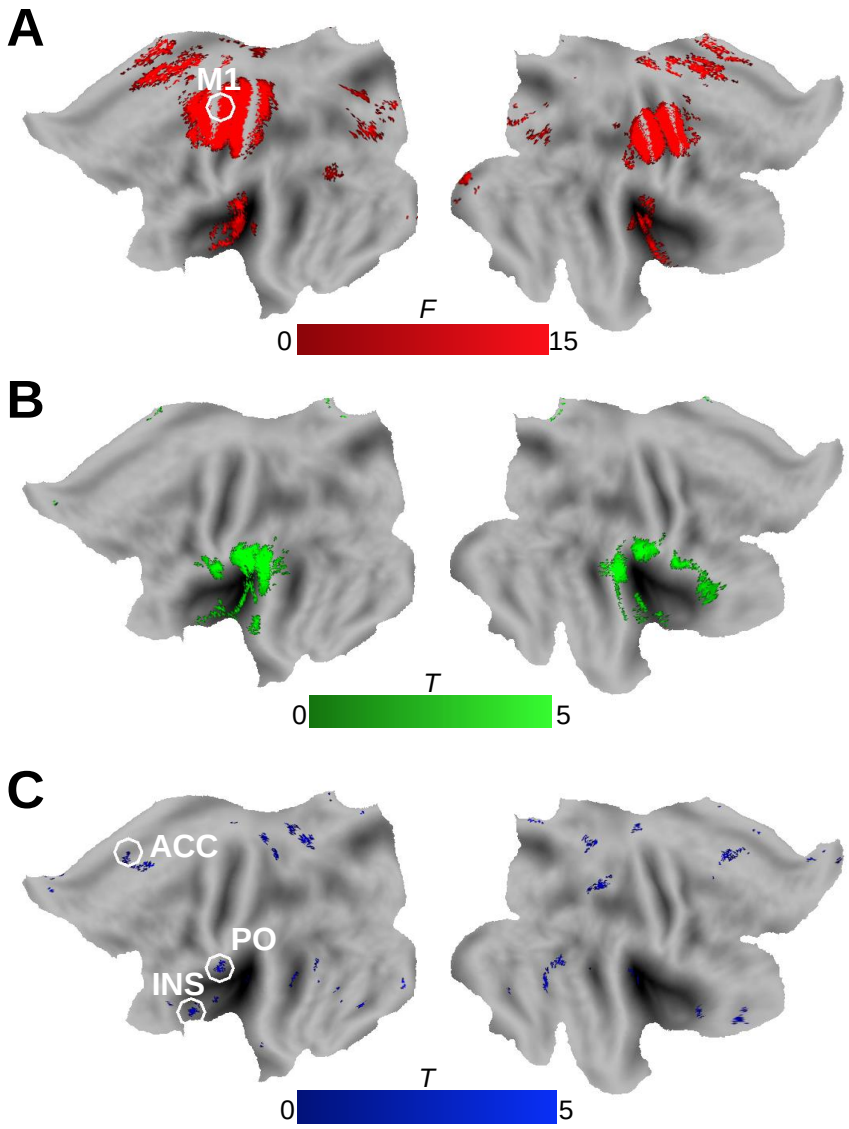
A
M1
F
0
15
B
T
0
5
C
ACC
PO
INS
T
0
5

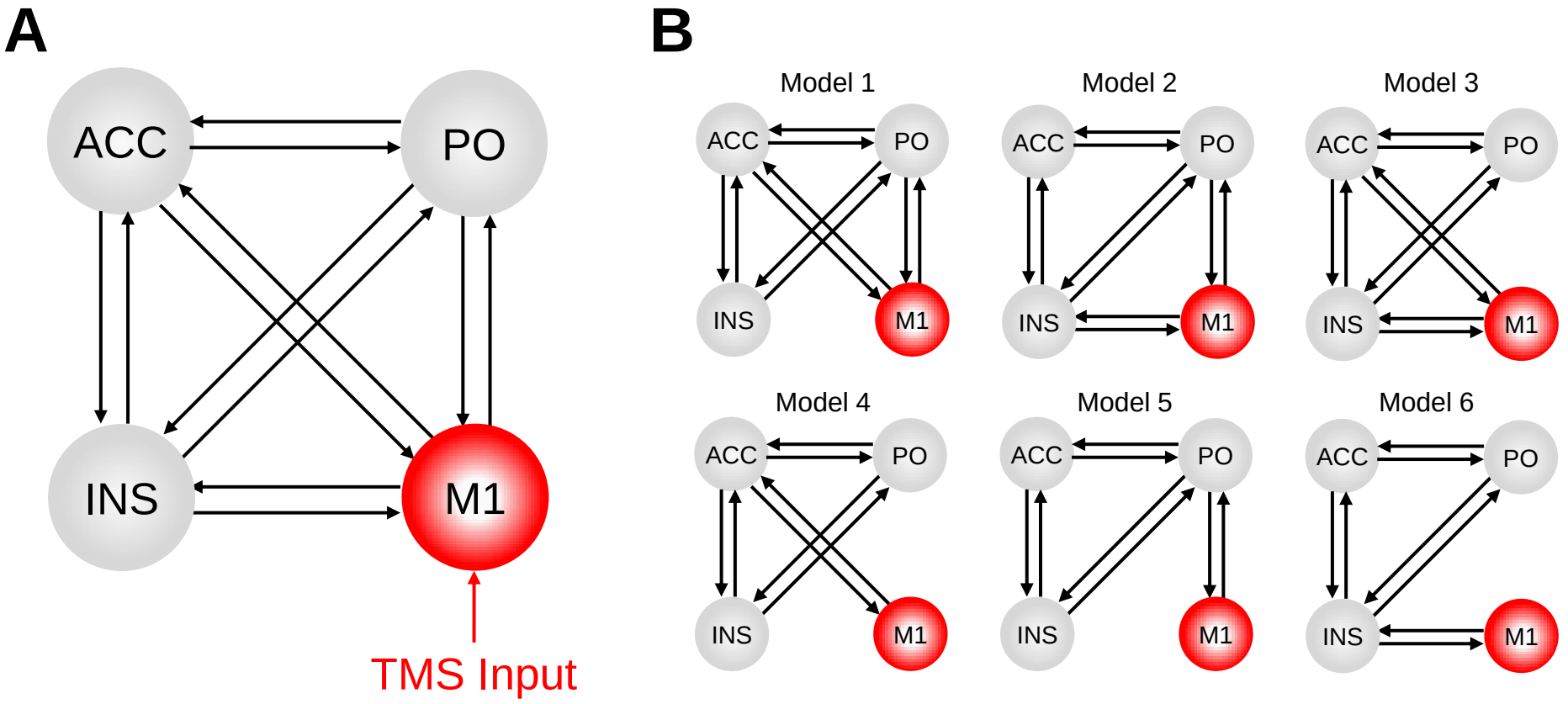
A
ACC
PO
INS
M1
TMS Input
B
Model 1
Model 2
Model 3
Model 4
Model 5
Model 6

A

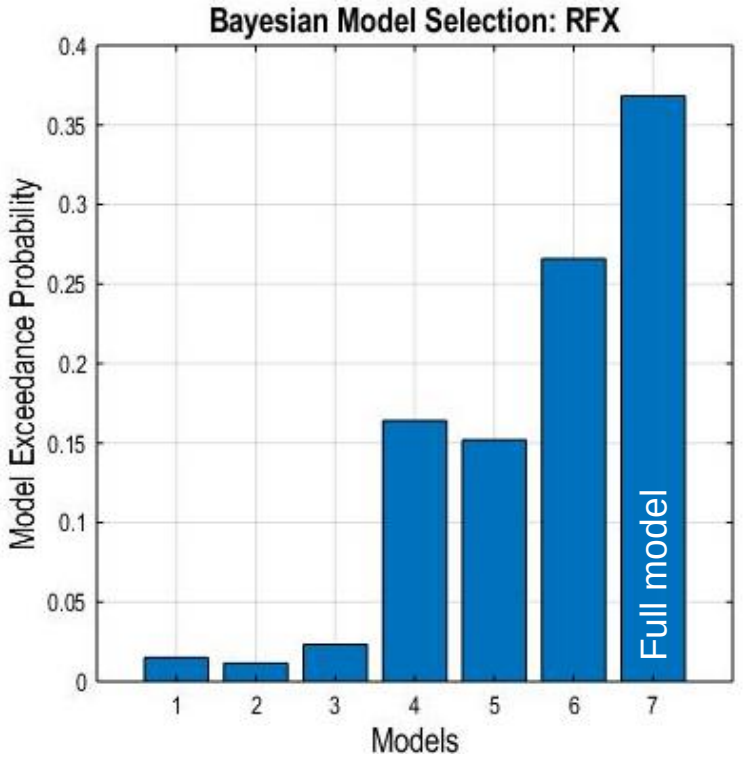
Bayesian Model Selection: RFX
Model Exceedance Probability
0.4
0.35
0.3
0.25
0.2
0.15
0.1
0.05
0
1
2
3
4
5
6
7
Models
Full model

B

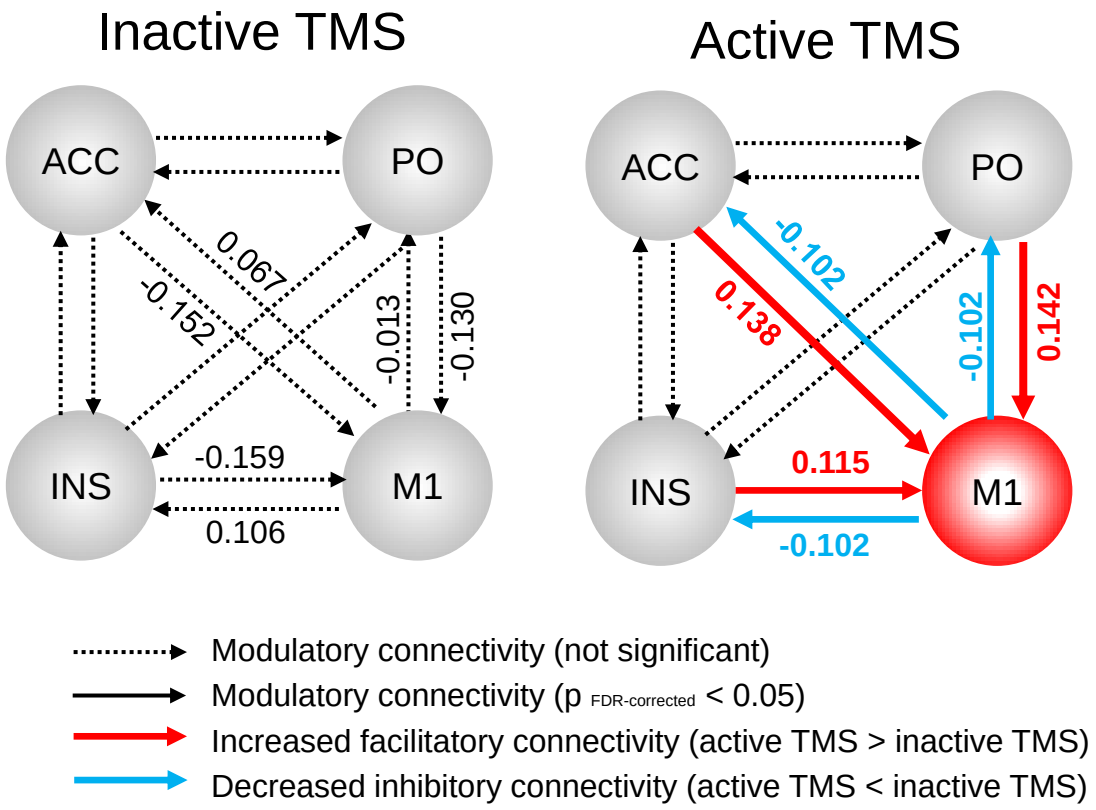
Inactive TMS
ACC
PO
INS
M1
0.067
-0.152
-0.013
-0.130
-0.159
0.106
Active TMS
ACC
PO
INS
M1
-0.102
0.138
-0.102
0.142
0.115
-0.102
Modulatory connectivity (not significant)
Modulatory connectivity (p FDR-corrected < 0.05)
Increased facilitatory connectivity (active TMS > inactive TMS)
Decreased inhibitory connectivity (active TMS < inactive TMS)

A

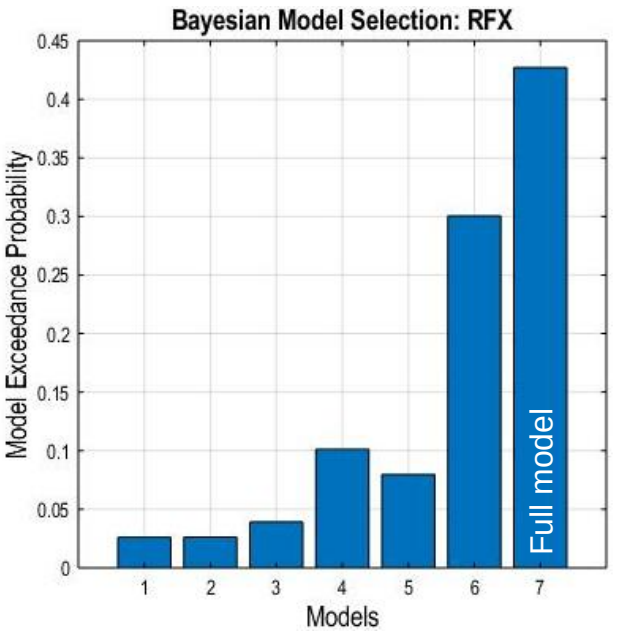
Bayesian Model Selection: RFX
Model Exceedance Probability
0.45
0.4
0.35
0.3
0.25
0.2
0.15
0.1
0.05
0
1
2
3
4
5
6
7
Models
Full model

B

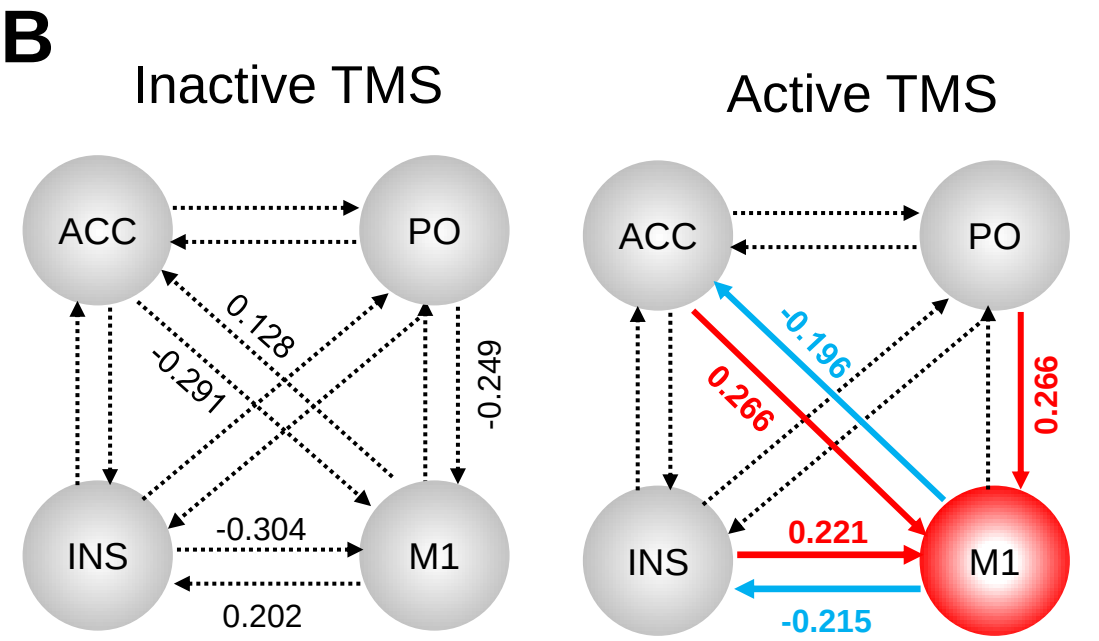
Inactive TMS
ACC
PO
INS
M1
0.128
-0.291
-0.249
-0.304
0.202
Active TMS
ACC
PO
INS
M1
-0.196
0.266
0.266
0.221
-0.215

C

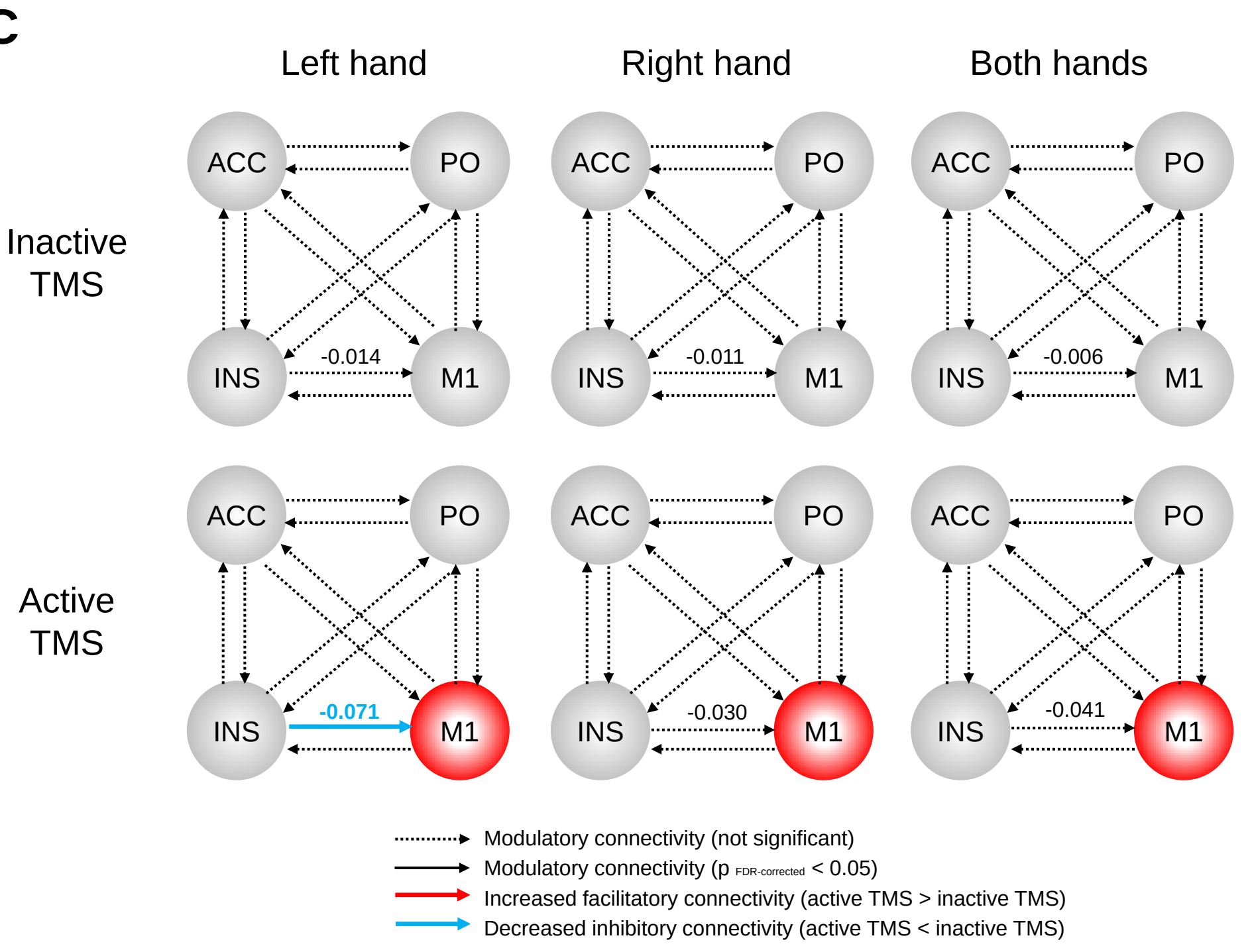
Left hand
Right hand
Both hands
Inactive TMS
Active TMS
ACC
PO
INS
M1
-0.014
-0.011
-0.006
-0.071
-0.030
-0.041
Modulatory connectivity (not significant)
Modulatory connectivity (p FDR-corrected < 0.05)
Increased facilitatory connectivity (active TMS > inactive TMS)
Decreased inhibitory connectivity (active TMS < inactive TMS)

A

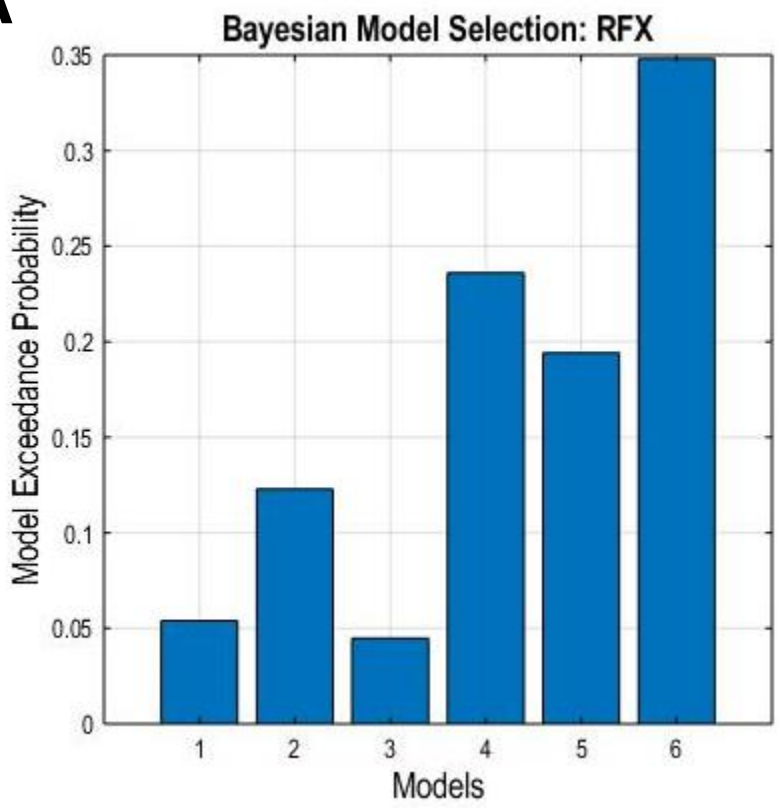
Bayesian Model Selection: RFX
Model Exceedance Probability
0.35
0.3
0.25
0.2
0.15
0.1
0.05
0
1
2
3
4
5
6
Models

B

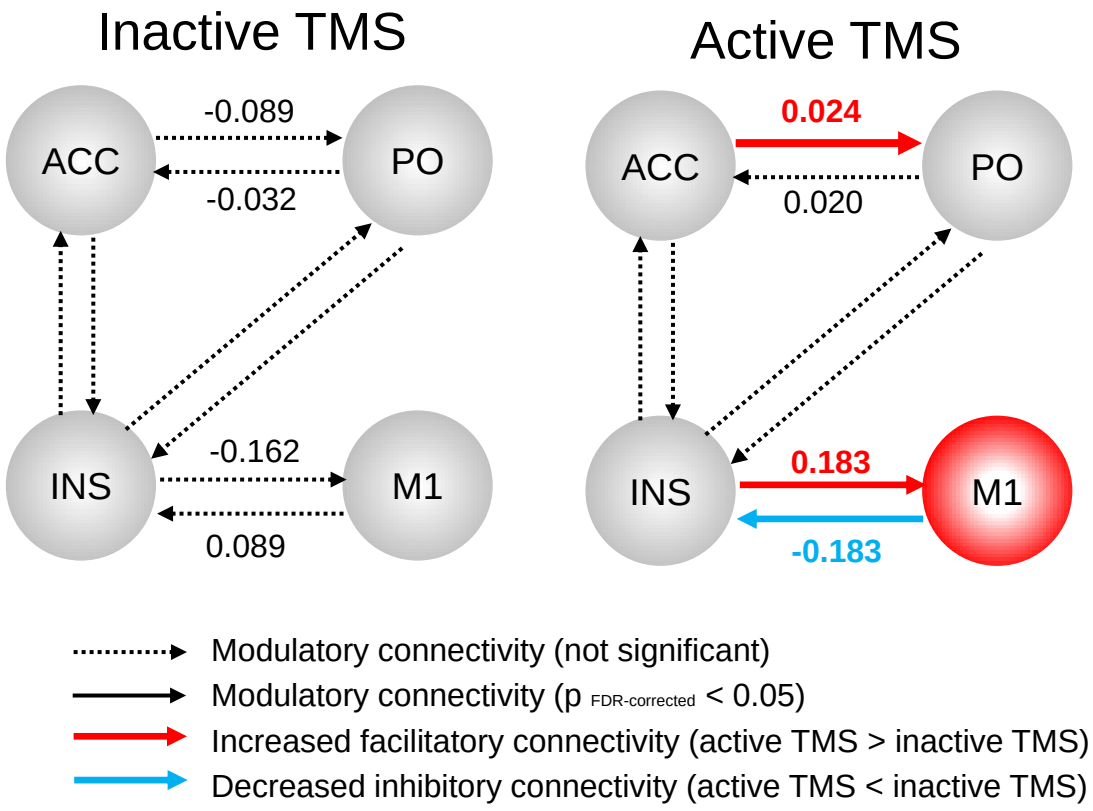
Inactive TMS
ACC
PO
-0.089
-0.032
INS
M1
-0.162
0.089
Active TMS
ACC
PO
0.024
0.020
INS
M1
0.183
-0.183
Modulatory connectivity (not significant)
Modulatory connectivity (p FDR-corrected < 0.05)
Increased facilitatory connectivity (active TMS > inactive TMS)
Decreased inhibitory connectivity (active TMS < inactive TMS)

A

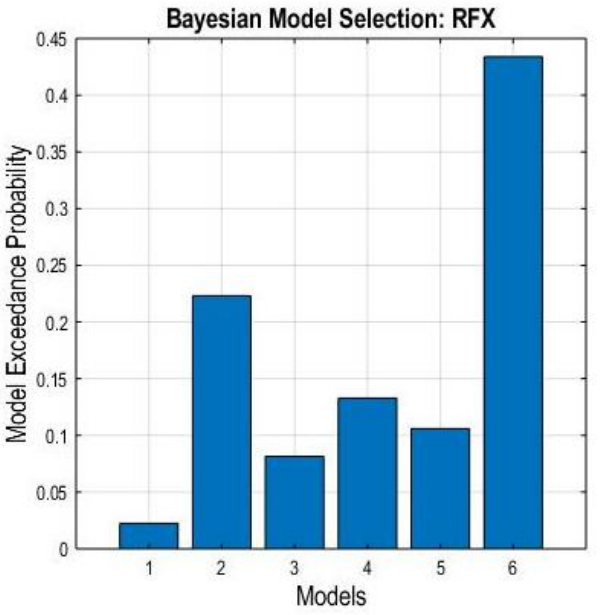

B

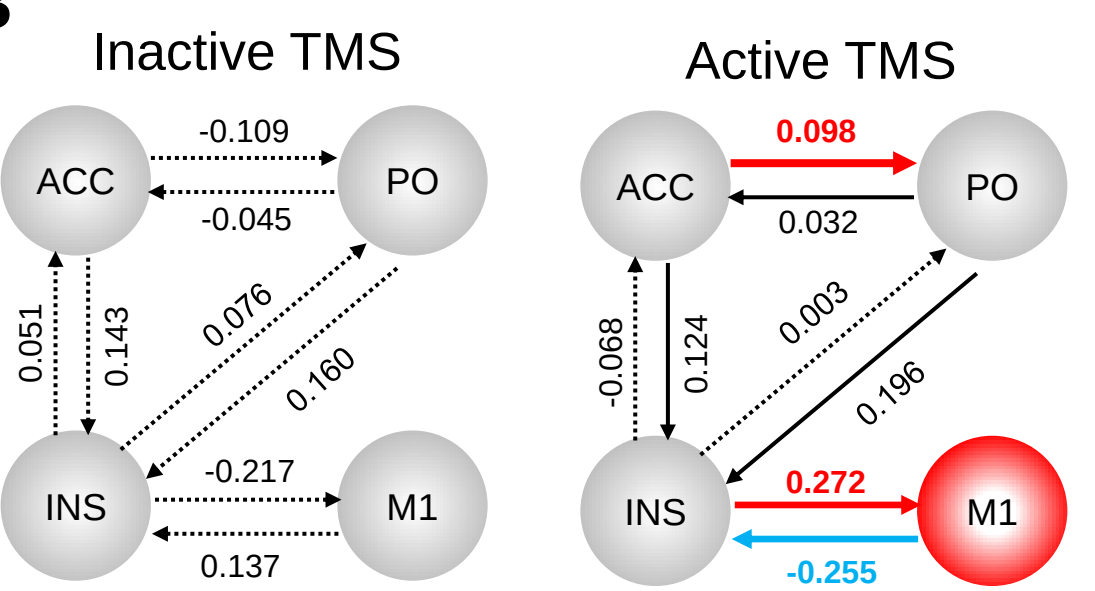

C

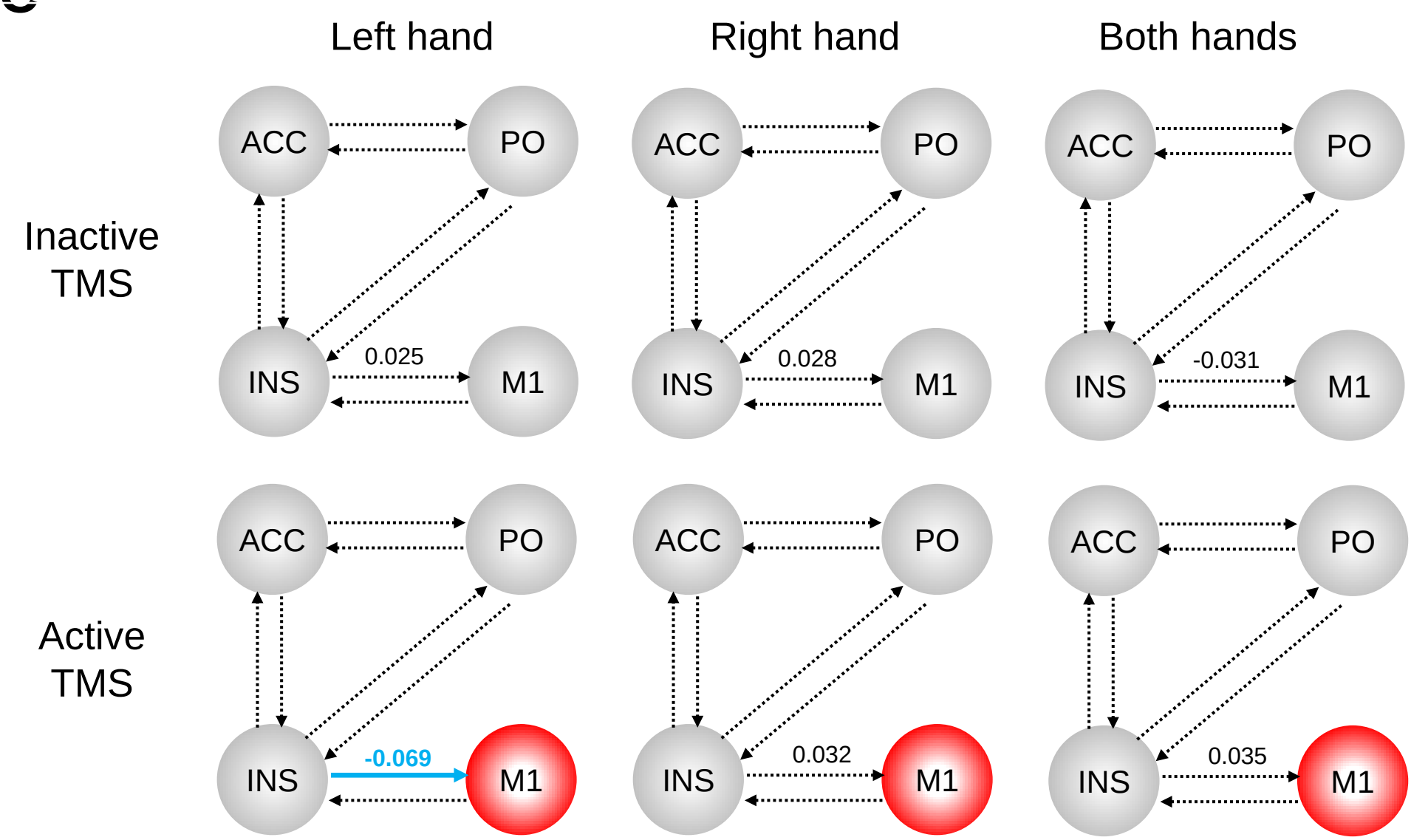

Modulatory connectivity (not significant)

Modulatory connectivity ($p_{FDR\text{-}corrected} < 0.05$)

Increased facilitatory connectivity (active TMS > inactive TMS)

Decreased inhibitory connectivity (active TMS < inactive TMS)

Dynamic Causal modeling

model selection

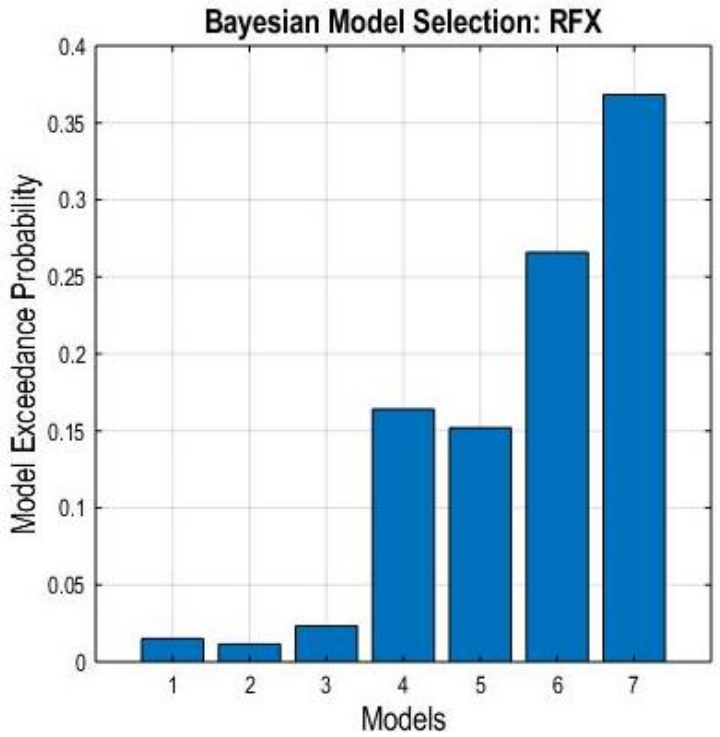

model space
(winning model)